Eur. Phys. J. C (2023) 83:783
https://doi.org/10.1140/epjc/s10052-023-11959-0

THE EUROPEAN PHYSICAL JOURNAL C

Regular Article - Theoretical Physics

The evolution of the primordial curvature perturbation in the ultraslow-roll inflation

Hao-Ran Zhao, Yi-Chen Liu, Ji-Xiang Zhao, Nan Li[a]

Department of Physics, College of Sciences, Northeastern University, Shenyang 110819, China

Received: 26 June 2023 / Accepted: 25 August 2023

Abstract A plateau on the background inflaton potential can lead inflation into the ultraslow-roll (USR) stage, during which the primordial curvature perturbation $\mathscr{R}$ can still remarkably evolve outside the horizon. In this paper, the evolution of the Fourier mode $\mathscr{R}_k$ and the resulting power spectrum $\mathscr{P}_{\mathscr{R}}(k)$ are systematically investigated. It is found that, when a scale crosses the horizon well before or after the USR stage, $\mathscr{R}_k$ only revolves around the origin in the complex plane. In contrast, if a scale crosses the horizon around the start of the USR stage, the argument of $\mathscr{R}_k$ will be nearly frozen and $\mathscr{R}_k$ will have a subsequent linear evolution accordingly, in which it may stop rather near or extremely far away from the origin, naturally explaining the entire growing stage of $\mathscr{P}_{\mathscr{R}}(k)$ on small scales from the minimum to the peak. Moreover, there is a sharp dip in $\mathscr{P}_{\mathscr{R}}(k)$, but the lowest point cannot reach 0 exactly. Our work provides a whole picture for $\mathscr{R}_k$ and $\mathscr{P}_{\mathscr{R}}(k)$ in the USR inflation and will help our understanding of the relevant primordial black hole and gravitational wave physics.

1 Introduction

The detection of gravitational waves from the merger of binary black holes marked the new epoch of multimessenger astronomy [1]. The characteristics of these black holes, such as their unexpectedly large masses and relatively small spins, suggest that they may not be usual astrophysical ones, but are of primordial origin [2–4]. Primordial black holes (PBHs) are formed before big bang nucleosynthesis, so they are a powerful probe in the early Universe [5]). At the same time, the first-order scalar perturbations that generate PBHs can also serve as the source of the second-order scalar-induced gravitational waves (SIGWs) [6,7]. Today, the Hawking radiation from PBHs can change the background intensities of various cosmic rays [8]. Moreover, PBHs are a natural and promising candidate of dark matter (DM) [9,10], and can act as the seeds of supermassive black holes in galactic centers [11], supported by the recent observation of the James Webb Space Telescope on the massive galaxies at high redshifts [12].

Different from astrophysical black holes, the mass range of PBHs can span almost 50 orders of magnitude, from the Planck mass to supermassive scale (10^{-38}–10^{10} $M_\odot$, with $M_\odot = 1.989 \times 10^{30}$ kg being the solar mass). Because of the Hawking radiation, the PBHs with mass $M < 5 \times 10^{-19}\, M_\odot$ have already evaporated, but the PBHs with mass $M > 5 \times 10^{-19}\, M_\odot$ can still exist today, acting as a stable and pressureless candidate of DM. The PBH abundance $f_{\rm PBH}$ is defined as its proportion in DM today. If $f_{\rm PBH} \gtrsim 0.1$, the PBHs can be considered as an effective candidate of DM; if $f_{\rm PBH} \ll 10^{-3}$, its possibility as DM can be safely excluded in the relevant mass range. Albeit various constraints from evaporation, lensing, dynamics, accretion, and gravitational waves have strictly constrained the upper bounds of $f_{\rm PBH}$ in different mass ranges, there remains an open mass window from $10^{-17}\, M_\odot$ (asteroid mass range) to $10^{-13}\, M_\odot$ (sublunar mass range), where PBHs are possible to compose all DM. For more recent and complete constraints on $f_{\rm PBH}$, see Refs. [8–10] and the references therein.

The PBH abundance $f_{\rm PBH}$ can be calculated from the power spectrum $\mathscr{P}_{\mathscr{R}}(k)$ of the primordial curvature perturbation $\mathscr{R}$ via the Press–Schechter theory [13] or the more general peak theory [14,15]. If $f_{\rm PBH} \sim 0.1$, $\mathscr{R}$ must be large enough, so that $\mathscr{P}_{\mathscr{R}}(k)$ can be significantly enhanced on small scales (e.g., 10^8–10^{18} Mpc^{-1}), with a peak up to $\mathscr{O}(10^{-2})$ at least. However, such a large magnitude cannot be achieved in the usual single-field slow-roll (SR) inflation models, which only generate a nearly scale-invariant power spectrum on large scales. For example, $\mathscr{P}_{\mathscr{R}}(k) \sim \mathscr{O}(10^{-9})$ on the scale of cosmic microwave background [16]. There-

[a] e-mail: linan@mail.neu.edu.cn (corresponding author)

Published online: 05 September 2023

fore, in order to produce abundant PBHs, the SR conditions must be violated on small scales, and this can be realized in the so-called ultraslow-roll (USR) inflation models [17–55].

The aim of this paper is to study the evolution of the primordial curvature perturbation $\mathscr{R}$ and the resulting power spectrum $\mathscr{P}_{\mathscr{R}}(k)$ both theoretically and numerically. Although the shape and amplitude of $\mathscr{P}_{\mathscr{R}}(k)$ have been obtained in various USR inflation models, there remain several important but unclear issues not thoroughly explored before [56,57]. For instance, there is always a sharp dip in $\mathscr{P}_{\mathscr{R}}(k)$ before its steep growth. Of course, the detail of this dip does not affect the PBH abundance and SIGW spectrum, as they are relevant only to the peak of $\mathscr{P}_{\mathscr{R}}(k)$. In Refs. [58–66], the location of the dip was calculated numerically or semi-analytically, but the underlying physical explanation seems still lacking.

In this paper, we will provide a new perspective on the evolution of $\mathscr{R}$ in the USR inflation. Our main improvements to previous works are threefold. First, we investigate the Fourier mode $\mathscr{R}_k$ and its derivative $\mathscr{R}_{k,N}$ with respect to the number of e-folds N in the complex plane. In this way, the entire growing stage of $\mathscr{P}_{\mathscr{R}}(k)$ from the dip to the peak is demonstrated as a natural consequence from an interesting linear evolution of $\mathscr{R}_k$. Second, by illustrating the evolutions of θ_k and φ_k (i.e., the arguments of $\mathscr{R}_k$ and $\mathscr{R}_{k,N}$), we confirm the linear evolution of $\mathscr{R}_k$, indicating that it is the argument θ_k rather than the modulus $|\mathscr{R}_k|$ that is frozen once the relevant scale crosses the horizon in the USR inflation. Third, we carefully study the minimum of $\mathscr{P}_{\mathscr{R}}(k)$ in the dip and find that it cannot reach 0 exactly, which is also seldom mentioned before. Altogether, we wish to give a whole picture and thorough understanding of $\mathscr{R}_k$ and $\mathscr{P}_{\mathscr{R}}(k)$, which will be beneficial to the model building of the USR inflation and help our research on PBH and gravitational wave physics.

Below, we will follow our previous works on the USR inflation [38,39,53], in which we considered an antisymmetric perturbation δV on the background inflaton potential $V_{\rm b}$ in the USR region. There are several advantages in such a construction. First, the USR stage can be separately studied from the SR stage, so it does not spoil the nearly scale-invariant $\mathscr{P}_{\mathscr{R}}(k)$ on large scales. Second, δV can be connected to $V_{\rm b}$ very smoothly on both sides of the USR region, and the inflaton can certainly surmount the perturbation. Third, there is no modulated oscillation in $\mathscr{P}_{\mathscr{R}}(k)$, avoiding the overproduction of tiny PBHs. Consequently, the fine-tuning problem frequently met in PBH physics can be largely relieved. In one word, the antisymmetric δV can create a plateau flat enough on $V_{\rm b}$, inducing a sufficiently long duration of the USR stage, in which $\mathscr{P}_{\mathscr{R}}(k)$ can be greatly enhanced.

This paper is organized as follows. In Sect. 2, we show the basic equation of motion for the primordial curvature perturbation $\mathscr{R}_k$ and study its power spectrum $\mathscr{P}_{\mathscr{R}}(k)$ in the USR inflation. In Sect. 3, the evolutions of $\mathscr{R}_k$ for five typical scales with different times of horizon-exit are systematically investigated in the complex plane. The resulting $\mathscr{P}_{\mathscr{R}}(k)$ is presented in Sect. 4, and several notable features in $\mathscr{P}_{\mathscr{R}}(k)$ are also explained in detail. We conclude in Sect. 5. We work in the natural system of units and set $c = \hbar = k_{\rm B} = 1$.

2 Primordial curvature perturbation and power spectrum

In this section, we show the equation of motion for the primordial curvature perturbation $\mathscr{R}_k$ and discuss the basic property of its power spectrum $\mathscr{P}_{\mathscr{R}}(k)$.

2.1 Basic equations

We start from the single-field inflation model, with the inflaton minimally coupled to gravity, and the relevant action reads

$$S = \int \mathrm{d}^4x\,\sqrt{-g}\left[\frac{m_{\rm P}^2}{2}R - \frac{1}{2}\partial_\mu\phi\partial^\mu\phi - V(\phi)\right],$$

where ϕ is the inflaton field, $V(\phi)$ is its potential, R is the Ricci scalar, and $m_{\rm P} = 1/\sqrt{8\pi G}$ is the reduced Planck mass, respectively.

In the inflationary era, besides the cosmic time t, it is more convenient to utilize the number of e-folds N as the time variable in cosmic dynamics, which is defined as $\mathrm{d}N = H(t)\,\mathrm{d}t = \mathrm{d}\ln a$, with $a = e^N$ being the scale factor, and $H = \dot{a}/a$ being the Hubble expansion rate. In order to characterize the motion of the inflaton, two important parameters are introduced as

$$\varepsilon = -\frac{\dot{H}}{H^2} = \frac{\phi_{,N}^2}{2m_{\rm P}^2},$$
$$\eta = -\frac{\ddot{\phi}}{H\dot{\phi}} = \frac{\phi_{,N}^2}{2m_{\rm P}^2} - \frac{\phi_{,NN}}{\phi_{,N}}.$$

In the usual SR inflation, ε and $|\eta|$ are always much smaller than 1 and are thus named as the SR parameters. However, in the USR stage, both SR conditions can be broken, and their values may be greatly changed, leaving significant influences on cosmic evolution, PBH abundance, and SIGW spectrum.

In terms of the SR parameters, the Friedmann equation for cosmic expansion can be expressed as

$$H^2 = \frac{V}{(3-\varepsilon)m_{\rm P}^2},$$

and the Klein–Gordon equation for the inflaton field ϕ can be written as

$$\phi_{,NN} + (3-\varepsilon)\phi_{,N} + \frac{V_{,\phi}}{H^2} = 0. \tag{1}$$

2.2 Primordial curvature perturbation

Now, we turn to the perturbations on the background spacetime. In Newtonian gauge, the metric with the scalar perturbation Φ reads

$$\mathrm{d}s^2 = -(1+2\Phi)\,\mathrm{d}t^2 + a^2(1-2\Phi)\delta_{ij}\,\mathrm{d}x^i\mathrm{d}x^j.$$

Here, we neglect the vector perturbation and anisotropic stress, as they are irrelevant to PBH and SIGW physics. Furthermore, a more useful and gauge-invariant primordial curvature perturbation $\mathscr{R}$ is defined as

$$\mathscr{R} = \Phi + \frac{H}{\dot{\phi}}\,\delta\phi = \Phi + \frac{\delta\phi}{\phi_{,N}},$$

and the equation of motion for its Fourier mode $\mathscr{R}_k$ is the Mukhanov–Sasaki (MS) equation [67,68],

$$\mathscr{R}_{k,NN} + (3+\varepsilon-2\eta)\mathscr{R}_{k,N} + \frac{k^2}{H^2e^{2N}}\mathscr{R}_k = 0. \tag{2}$$

The initial conditions of the MS equation can be fixed by the Bunch–Davies vacuum condition [69]. In the very early Universe, the asymptotic solution of $\mathscr{R}_k$ is [70]

$$\mathscr{R}_k = \frac{e^{ik/(He^N)}}{z\sqrt{2k}}\left(1 + \frac{iHe^N}{k}\right), \tag{3}$$

where $z = a\dot{\phi}/H = \phi_{,N}e^N$.[1] Hence, in the very early stage of inflation when $k \gg aH = He^N$, from Eq. (3), we have

$$\mathscr{R}_k\Big|_{N\to N_{\rm ini}} = \frac{e^{ik/(He^N)}}{z\sqrt{2k}}, \tag{4}$$

$$\mathscr{R}_{k,N}\Big|_{N\to N_{\rm ini}} = -\frac{e^{ik/(He^N)}}{z\sqrt{2k}}\left(\frac{z_{,N}}{z} + \frac{ik}{He^N}\right), \tag{5}$$

where $N_{\rm ini}$ is the initial number of e-folds. For convenience of the numerical calculations in Sect. 3, it is sufficient to set

$$N_{\rm ini} = N_{\rm out} - 7,$$

where $N_{\rm out}$ is the number of e-folds when the relevant scale k crosses the horizon (i.e., $k = a(N_{\rm out})H(N_{\rm out}) = H(N_{\rm out})e^{N_{\rm out}}$).

Moreover, we can further decompose $\mathscr{R}_k$ in the complex plane as

$$\mathscr{R}_k = |\mathscr{R}_k|e^{-i\theta_k}, \tag{6}$$

where $|\mathscr{R}_k|$ and θ_k are the modulus and argument of $\mathscr{R}_k$. Substituting Eq. (6) into Eq. (2), we obtain the equation of motion for $|\mathscr{R}_k|$ as

$$|\mathscr{R}_k|_{,NN} + (3+\varepsilon-2\eta)|\mathscr{R}_k|_{,N} + \frac{k^2}{H^2e^{2N}}\left(1 - \frac{1}{4z^4k^2|\mathscr{R}_k|^4}\right)|\mathscr{R}_k| = 0. \tag{7}$$

From Eq. (4), the initial conditions of Eq. (7) read

$$|\mathscr{R}_k|\Big|_{N\to N_{\rm ini}} = -\frac{1}{z\sqrt{2k}}, \tag{8}$$

$$|\mathscr{R}_k|_{,N}\Big|_{N\to N_{\rm ini}} = \frac{z_{,N}}{z^2\sqrt{2k}}. \tag{9}$$

In general, the inflaton ϕ rolls down from its potential $V(\phi)$, so $z = \phi_{,N}e^N < 0$ when $N \to N_{\rm ini}$. Considering the positivity of $|\mathscr{R}_k|$, we have assigned a negative sign in Eq. (8). Next, taking into account the asymptotic solutions in Eqs. (4) and (5), we obtain the relation between θ_k and $|\mathscr{R}_k|$ as

$$\theta_{k,N} = \frac{1}{2z^2He^N|\mathscr{R}_k|^2}. \tag{10}$$

Furthermore, the derivative of $\mathscr{R}_k$ can also be decomposed as

$$\mathscr{R}_{k,N} = |\mathscr{R}_{k,N}|e^{-i\varphi_k},$$

where the argument φ_k can be obtained from Eq. (6) as

$$\varphi_k = \arctan\frac{|\mathscr{R}_k|\theta_{k,N}}{|\mathscr{R}_k|_{,N}} + \theta_k + n\pi \quad (n\in\mathbb{Z}). \tag{11}$$

Substituting Eq. (10) into Eq. (11), after some algebra, we obtain

$$\varphi_{k,N} = \frac{1}{2z^2He^N|\mathscr{R}_k|^2} - \frac{(2z^2He^N|\mathscr{R}_k||\mathscr{R}_k|_{,N})_{,N}}{(2z^2He^N|\mathscr{R}_k||\mathscr{R}_k|_{,N})^2+1}. \tag{12}$$

The influences of θ_k and φ_k on the evolution of $\mathscr{R}_k$ will be explored in Sect. 3.3.

[1] In Ref. [70], $\mathscr{R}_k$ is given in terms of the conformal time τ as

$$\mathscr{R}_k = \frac{e^{-ik\tau}}{z\sqrt{2k}}\left(1 - \frac{i}{k\tau}\right),$$

where $\mathrm{d}\tau = \mathrm{d}t/a = \mathrm{d}N/(He^N)$, and $a = -1/(H\tau) = e^N$.

2.3 Power spectrum

The statistical property of cosmological perturbations can be encoded in the two-point correlation function or equivalently the power spectrum in the Fourier space. The dimensionless power spectrum $\mathscr{P}_{\mathscr{R}}(k)$ of the primordial curvature perturbation $\mathscr{R}_k$ is defined as

$$\mathscr{P}_{\mathscr{R}}(k) = \frac{k^3}{2\pi^2}|\mathscr{R}_k|^2\Big|_{k\ll aH}.$$

In the SR inflation, $\mathscr{R}_k$ becomes almost frozen once the scale k crosses the horizon, so $\mathscr{P}_{\mathscr{R}}(k)$ can be effectively calculated at $k = aH$ for simplicity. However, in the USR inflation, $\mathscr{R}_k$ can still significantly evolve after the horizon-exit, so $\mathscr{P}_{\mathscr{R}}(k)$ must be evaluated at the end of inflation when $k \ll aH$.

In the SR inflation, on large scales, $\mathscr{P}_{\mathscr{R}}(k)$ can be usually formulated in a power-law form as $\mathscr{P}_{\mathscr{R}}(k) = A_{\rm s}(k/k_*)^{n_{\rm s}-1}$, where k_* is the pivot scale, $A_{\rm s}$ is the amplitude of $\mathscr{P}_{\mathscr{R}}(k)$ at k_*, and $n_{\rm s}$ is the scalar spectral index, respectively. Moreover, $n_{\rm s}$ and the tensor-to-scalar ratio r can be expressed in terms of the SR parameters as $n_{\rm s} = 1 - 4\varepsilon + 2\eta$ and $r = 16\varepsilon$. In the Planck satellite experiment, on the pivot scale $k_* = 0.05\ {\rm Mpc}^{-1}$, we have the central values $A_{\rm s} = 2.10 \times 10^{-9}$ and $n_{\rm s} = 0.965\pm0.008$, and also $r < 0.06$ at 95% confidence level [16].

However, on small scales where PBHs and SIGWs are expected, the constraints on $\mathscr{P}_{\mathscr{R}}(k)$ are still rather loose [5,8–10] (the observation of cosmic microwave background only covers about 10 e-folds on large scales). In the USR inflation, if there exist PBHs with considerable abundance $f_{\rm PBH} \sim 0.1$, $\mathscr{P}_{\mathscr{R}}(k)$ must possess a peak up to $\mathscr{O}(10^{-2})$ on small scales. In addition, $n_{\rm s} - 1$ is approximately equal to 4 in the growing stage of $\mathscr{P}_{\mathscr{R}}(k)$ [31,58,61], and there is even a sharp dip before the steep growth of $\mathscr{P}_{\mathscr{R}}(k)$, all to be discussed in Sect. 4.

3 Evolution of $\mathscr{R}_k$ in the complex plane

In this section, we first construct an USR inflation model, with an antisymmetric perturbation on the background inflaton potential in the USR region. Then, the evolutions of $\mathscr{R}_k$ for five typical scales are systematically studied in the complex plane. Furthermore, these behaviors are reinterpreted by exploring the evolutions of the arguments θ_k and φ_k.

3.1 Model

Below, we choose the Kachru–Kallosh–Linde–Trivedi potential [71] as the background inflaton potential $V_{\rm b}(\phi)$,

$$V_{\rm b}(\phi) = V_0\frac{\phi^2}{\phi^2 + (m_{\rm P}/2)^2}.$$

Meanwhile, to lead inflation into the USR stage, a perturbation $\delta V(\phi)$ is introduced on $V_{\rm b}(\phi)$ as

$$\delta V(\phi) = -A\frac{\phi - \phi_0}{1 + (\phi - \phi_0)^2/(2\sigma^2)},$$

where three model parameters A, ϕ_0, and σ characterize the amplitude, position, and width of $\delta V(\phi)$, so $\delta V(\phi)$ is antisymmetric around ϕ_0. (The specific form of $\delta V(\phi)$ is not unique, and other kinds of $\delta V(\phi)$ can be found in Refs. [38,39,53].) Thus, the total inflaton potential reads $V(\phi) = V_{\rm b}(\phi) + \delta V(\phi)$. For simplicity, we set $A = V_{{\rm b},\phi}(\phi_0)$. In this way, there can be a perfect plateau at ϕ_0. Following Ref. [39], we choose $V_0/m_{\rm P}^4 = 10^{-10}$, $\phi_0/m_{\rm P} = 1.31$, and $\sigma/m_{\rm P} = 0.0831881$. With these parameters, there can be PBHs of $10^{-17}M_\odot$ with abundance $f_{\rm PBH} \sim 0.1$. Moreover, we set the initial conditions of Eq. (1) as $\phi/m_{\rm P} = 3.30$ and $\phi_{,N}/m_{\rm P} = -0.0137$, so that $\mathscr{P}_{\mathscr{R}}(k)$ is nearly scale-invariant on the pivot scale k_*, with an appropriate $n_{\rm s} = 0.959$ and a relatively small $r = 0.0032$, both satisfying the Planck constraints [16].

By numerically solving the Friedmann and Klein–Gordon equations, we obtain the two parameters ε and η throughout inflation. In the SR stage, ε and $|\eta|$ are both much smaller than 1 and vary smoothly. In contrast, during the USR stage, their values change dramatically and may even approach $\mathscr{O}(1)$, as shown in Fig. 1. The starting and ending points of the USR stage are determined by

$$\eta(N_{\rm s}) = \eta(N_{\rm e}) = 0.$$

With the model parameters listed above, we have

$$N_{\rm s} = 56.81, \quad N_{\rm e} = 60.93.$$

3.2 Evolution of $\mathscr{R}_k$

Now, we start to investigate the evolution of the primordial curvature perturbation $\mathscr{R}_k$. Since $\mathscr{R}_k$ is complex, we need to numerically solve the MS equation in the complex plane, in which $|\mathscr{R}_k|$ indicates the distance from the origin to the position of $\mathscr{R}_k$, and $|\mathscr{R}_{k,N}|$ is the speed of motion of $\mathscr{R}_k$. In the following, the evolutions of $|\mathscr{R}_k|$ and $|\mathscr{R}_{k,N}|$ are systematically studied for five typical scales, for which the numbers of e-folds when they cross the horizon are

$$N_{\rm out} = 50,\ 52.89,\ 55,\ 58.84,\ 62.$$

The reason for choosing these numbers is that they correspond to five typical positions in the power spectrum

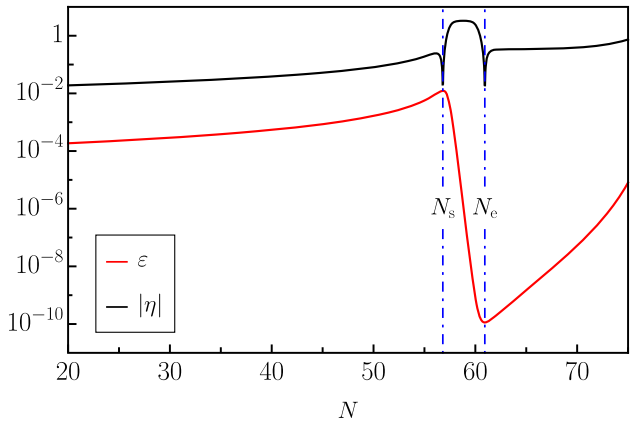

Fig. 1 The evolutions of ε and $|\eta|$ as a function of the number of e-folds N. In the early SR stage, $\varepsilon \sim \mathcal{O}(10^{-4})$, and $|\eta| \sim \mathcal{O}(10^{-2})$. The starting and ending points of the USR stage are determined by $\eta(N_s) = \eta(N_e) = 0$, with $N_s = 56.81$ and $N_e = 60.93$. In the USR stage, ε drops almost exponentially, and $|\eta|$ may even reach $\mathcal{O}(1)$

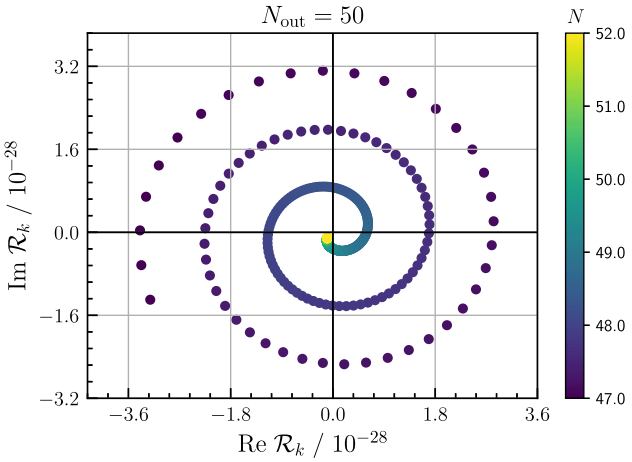

Fig. 3 The evolution of $\mathscr{R}_k$ from $N = 47$ to 52 for the scale with $N_{\rm out} = 50$. The horizontal and vertical axes are the real and imaginary parts of $\mathscr{R}_k$, respectively. The number of e-folds N is illustrated in color, and the difference ΔN between two adjacent dots is set to be 0.01. In the complex plane, $\mathscr{R}_k$ revolves clockwise around the origin and eventually stagnates near it. Also, it decelerates monotonically, as the interval between the dots decreases from outside to inside. This behavior indicates that, when $N_{\rm out}$ is much smaller than N_s, $|\mathscr{R}_k|$ is almost constant once the relevant scale crosses the horizon, and the influence from the USR stage is negligible

$\mathscr{P}_{\mathscr{R}}(k)$ (i.e., the nearly scale-invariant region, sharp dip, steep growth, peak, and falling stage, respectively, to be shown in Fig. 9). Our basic results are summarized in Fig. 2, and the detailed analysis of each case can be found in Figs. 3, 4, 5, 6 and 7.

Below, we analyze these five typical cases in order.

First, we consider the scale with $N_{\rm out} = 50$, which crosses the horizon much earlier than the start of the USR stage. In Fig. 3, the evolution of $\mathscr{R}_k$ from $N = 47$ to 52 is shown in the complex plane, and the difference of the number of e-folds between two adjacent dots is set to be $\Delta N = 0.01$. It can be observed that $\mathscr{R}_k$ revolves clockwise from outside to the origin and eventually stops near it. The interval between the dots gradually decreases from outside to inside, meaning that $\mathscr{R}_k$ decelerates monotonically, consistent with the trend of the black line before N_s in Fig. 2b. This can also be seen in Fig. 2a, in which $|\mathscr{R}_k|$ remains almost constant after $N_{\rm out}$, indicating that the USR stage has negligible effect on the large-scale curvature perturbation.

Second, we discuss an important and complicated case with $N_{\rm out} = 52.89$. In the present situation, the USR stage remarkably influences the evolution of $\mathscr{R}_k$, as shown in Fig. 4, with $N \in (50, 62.9)$. From Fig. 4a, in the early phase before

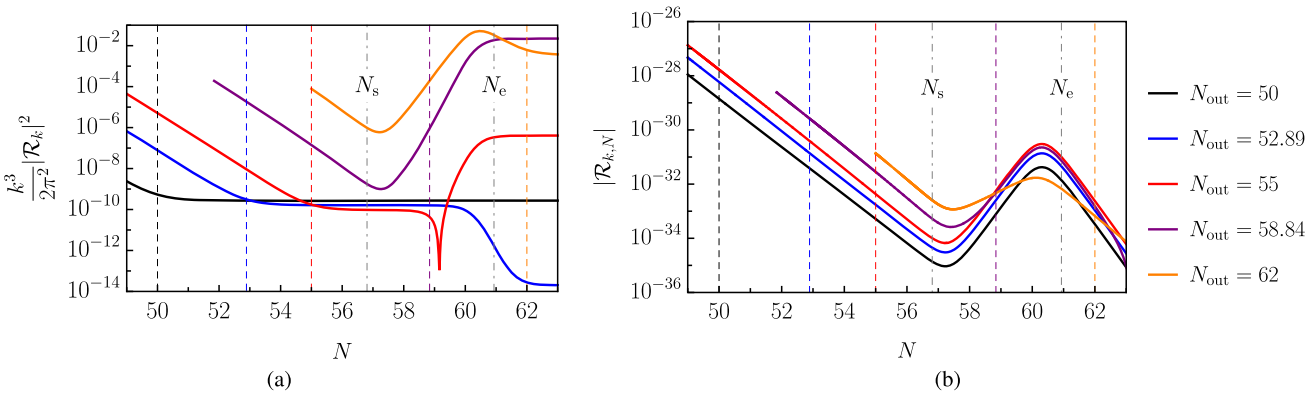

Fig. 2 The evolutions of $k^3|\mathscr{R}_k|^2/(2\pi^2)$ and $|\mathscr{R}_{k,N}|$ from $N = 49$ to 63 for five typical scales, with the numbers of e-folds when they cross the horizon being $N_{\rm out} = 50$ (black line), 52.89 (blue line), 55 (red line), 58.84 (purple line), and 62 (orange line), respectively. The vertical dashed lines indicate the different $N_{\rm out}$ for each case, with the same color as their corresponding curves. The starting and ending points of the USR stage are denoted by two gray dot-dashed lines, with $N_s = 56.81$ and $N_e = 60.93$. The initial point of each curve sets out at $N_{\rm ini} = N_{\rm out} - 7$ for numerical convenience

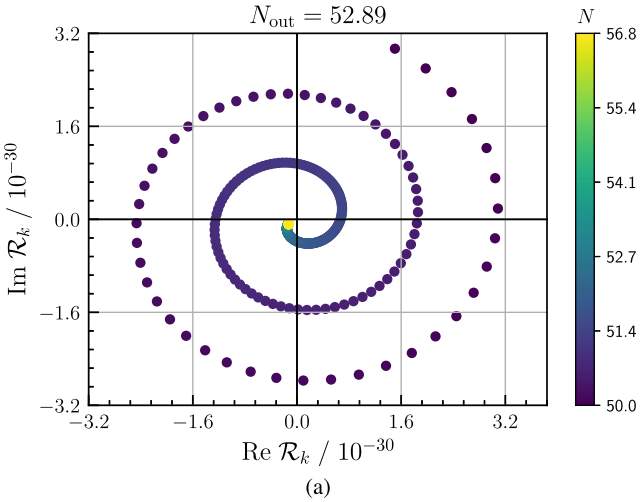

Fig. 4 The evolution of $\mathcal{R}_k$ from $N = 50$ to 62.9 for the scale with $N_{\rm out} = 52.89$. In Fig. 4a, before the USR stage, the evolution of $\mathcal{R}_k$ still resembles that in Fig. 3 ($\Delta N = 0.01$). In Fig. 4b, due to the influence of the USR stage, the horizontal and vertical coordinates of the dots are highly linearly correlated (from $N = 56.8$ to 62.9), with the Pearson correlation coefficient being 0.999999999999984 ($\Delta N = 0.1$). In this linear evolution, $\mathcal{R}_k$ eventually stops at a position extremely near the origin. This characteristic behavior causes a remarkable drop of $|\mathcal{R}_k|$ and thus explains the notable dip in $\mathcal{P}_{\mathcal{R}}(k)$

$N_{\rm s}$ (from $N = 50$ to 56.8), the behavior of $\mathcal{R}_k$ basically resembles that in Fig. 3. However, once the USR stage begins, $\mathcal{R}_k$ first stagnates for a fairly long time and then evolves along a perfectly straight line in the complex plane, as shown in Fig. 4b. During this unusual linear evolution from $N = 56.8$ to 62.9, $\mathcal{R}_k$ moves directly towards the origin and finally stops extremely near it, inducing a significant decrease of $|\mathcal{R}_k|$ (roughly between $N = 60$ and 62, as can also be seen in Fig. 2a). It is this decrease of $|\mathcal{R}_k|$ that naturally explains the notable dip in the power spectrum $\mathcal{P}_{\mathcal{R}}(k)$ in Fig. 9.

Third, we study the scale with $N_{\rm out} = 55$. This scale also crosses the horizon before $N_{\rm s}$, but there is a distinction from the former cases. The evolution of $\mathcal{R}_k$ from $N = 52$ to 65 is shown in Fig. 5. We clearly observe that the linear evolution at present is rather different from that in Fig. 4b. Instead of stopping near the origin, $\mathcal{R}_k$ first approaches the origin, then departs from it, and finally converges to a faraway position. This seemingly strange phenomenon can be understood as follows. From Fig. 2b, the speed $|\mathcal{R}_{k,N}|$ for the $N_{\rm out} = 55$ case (red line) is always larger than that for the $N_{\rm out} = 52.89$ case (blue line), and this is the essential reason why $\mathcal{R}_k$ moves farther now. Moreover, the behavior of $\mathcal{R}_k$ causes $|\mathcal{R}_k|$ to first fall and then rise again to an even higher value, as shown in the red line in Fig. 2a. This process occurs roughly from $N = 59$ to 61 and corresponds to the growing stage of $\mathcal{P}_{\mathcal{R}}(k)$ in Fig. 9.

Fourth, we discuss another special scale with $N_{\rm out} = 58.84$, which lies within the USR stage. In Fig. 6, we show the evolution of $\mathcal{R}_k$ from $N = 55.5$ to 62. Different from the three previous cases, $\mathcal{R}_k$ no longer approaches the origin. In

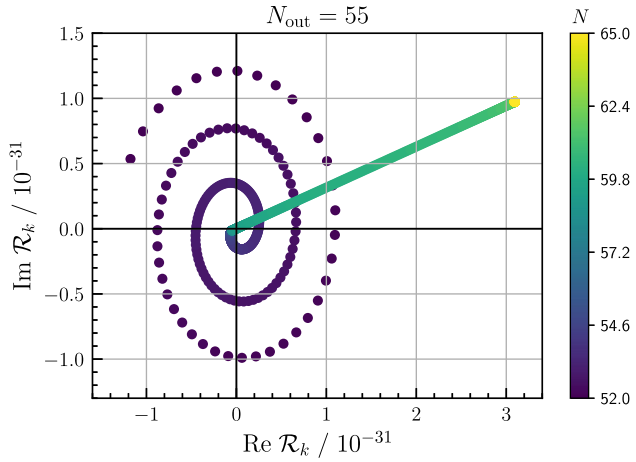

Fig. 5 The evolution of $\mathcal{R}_k$ from $N = 52$ to 65 for the scale with $N_{\rm out} = 55$ ($\Delta N = 0.01$). The Pearson correlation coefficient for the linear evolution process with $N \in (56, 65)$ is 0.99999999793965. Different from Fig. 4b, $\mathcal{R}_k$ no longer stops near the origin but at a faraway position, leading to the steep growth of $\mathcal{P}_{\mathcal{R}}(k)$. (It should be noted that the linear evolution does not intersect with the origin.)

fact, after the USR stage starts, $\mathcal{R}_k$ almost immediately enters the linear evolution but with a relatively large distance to the origin (see Fig. 6a) and eventually stops at an extremely distant point (see Fig. 6b), consistent with the trend of the purple line in Fig. 2. Consequently, the final value of $k^3|\mathcal{R}_k|^2/(2\pi^2)$ is the largest among all five cases, corresponding to the peak of $\mathcal{P}_{\mathcal{R}}(k)$ in Fig. 9.

Last, we set $N_{\rm out} = 62$, which is a typical case with the relevant scale crossing the horizon after the USR stage. We show the evolution of $\mathcal{R}_k$ in Fig. 7. Compared with the above

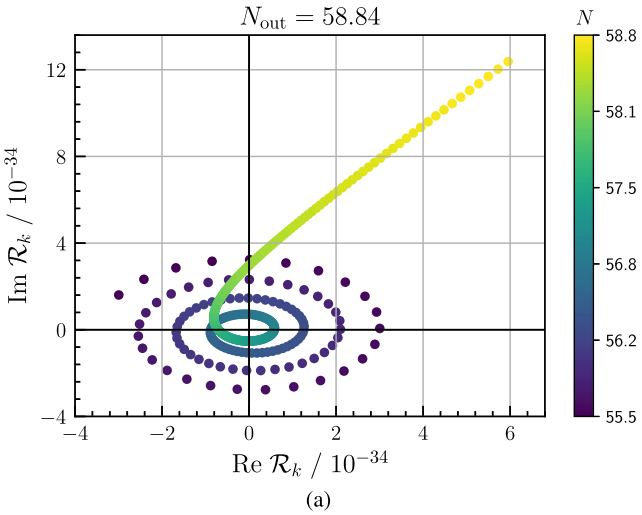

Fig. 6 The evolution of $\mathscr{R}_k$ from $N = 55.5$ to 62 for the case with $N_{\rm out} = 58.84$, with the relevant scale crossing the horizon within the USR stage. In Fig. 6a, $\mathscr{R}_k$ first revolves around the origin, but does not come very close to it any longer. With the beginning of the USR stage, $\mathscr{R}_k$ almost immediately starts the linear evolution ($\Delta N = 0.01$). The subsequent linear evolution from $N = 58.8$ to 62 is shown in Fig. 6b ($\Delta N = 0.05$), but the plotting scale is 1000 times that of Fig. 6a. Therefore, $\mathscr{R}_k$ finally stops at a position extremely far away from the origin, corresponding to the peak of $\mathscr{P}_{\mathscr{R}}(k)$. The Pearson correlation coefficient for the linear evolution process with $N \in (58.8, 62)$ is 0.999999996557677

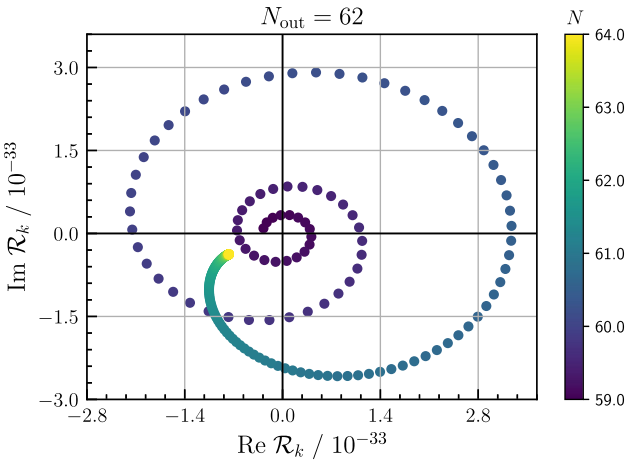

Fig. 7 The evolution of $\mathscr{R}_k$ from $N = 59$ to 64 for the case with $N_{\rm out} = 62$ ($\Delta N = 0.02$). The relevant scale crosses the horizon after the USR stage, and $\mathscr{R}_k$ finally approaches a position with a relatively large distance from the origin, without the subsequent linear evolution, corresponding to the falling stage of $\mathscr{P}_{\mathscr{R}}(k)$

four cases, the most distinguishing character here is that $\mathscr{R}_k$ first revolves away from the origin and then turn backwards, but it neither stagnates near the origin nor possesses a further linear evolution. As a result, $|\mathscr{R}_k|$ first increases, then decreases, and finally tends to a relatively large value. This can also be seen from the orange line in Fig. 2a and thus explains the falling stage of $\mathscr{P}_{\mathscr{R}}(k)$ in Fig. 9.

3.3 Evolutions of θ_k and φ_k

Below, we adopt a new point of view to reinterpret the evolution of $\mathscr{R}_k$, especially for its linear evolution process. In Fig. 8, we show $|\theta_{k,N}|$ and $|\varphi_{k,N}|$ (i.e., the time derivatives of the arguments of $\mathscr{R}_k$ and $\mathscr{R}_{k,N}$) as a function of N, which characterize the changes in the direction of motion of $\mathscr{R}_k$ and $\mathscr{R}_{k,N}$, respectively.

First, $\theta_{k,N}$ can be solved from Eqs. (7) and (10). In Fig. 8a, we observe that all $|\theta_{k,N}|$ drops before $N_{\rm s}$, meaning that the angular velocity of $\mathscr{R}_k$ around the origin decreases monotonically. When $N > N_{\rm s}$, the drop of $|\theta_{k,N}|$ continues for the small-scale cases with $N_{\rm out} = 58.84$ (purple line) and 62 (orange line). This means that the angular velocity of $\mathscr{R}_k$ keeps decreasing, and $\mathscr{R}_k$ will never be close to the origin, as can be seen in Figs. 6 and 7. However, for the large-scale cases with $N_{\rm out} = 50$ (black line), 52.89 (blue line), and 55 (red line), $|\theta_{k,N}|$ increases in the USR stage, and $\mathscr{R}_k$ can approach the origin, as shown in Figs. 3, 4 and 5. More interestingly, there is a cusp in the red line with $N_{\rm out} = 55$. This spiky behavior of $|\theta_{k,N}|$ induces a jump of nearly π for the argument θ_k, naturally indicating the linear evolution of $\mathscr{R}_k$ by the origin (but still with a tiny distance), totally in agreement with Fig. 5.

Similarly, $\varphi_{k,N}$ can be solved from Eqs. (7) and (12). In Fig. 8b, we clearly find that, except for the case with $N_{\rm out} = 62$ (orange line), all other $|\varphi_{k,N}|$ greatly decreases for a period of time during the USR stage, meaning that φ_k almost keeps constant in these cases. As φ_k describes the

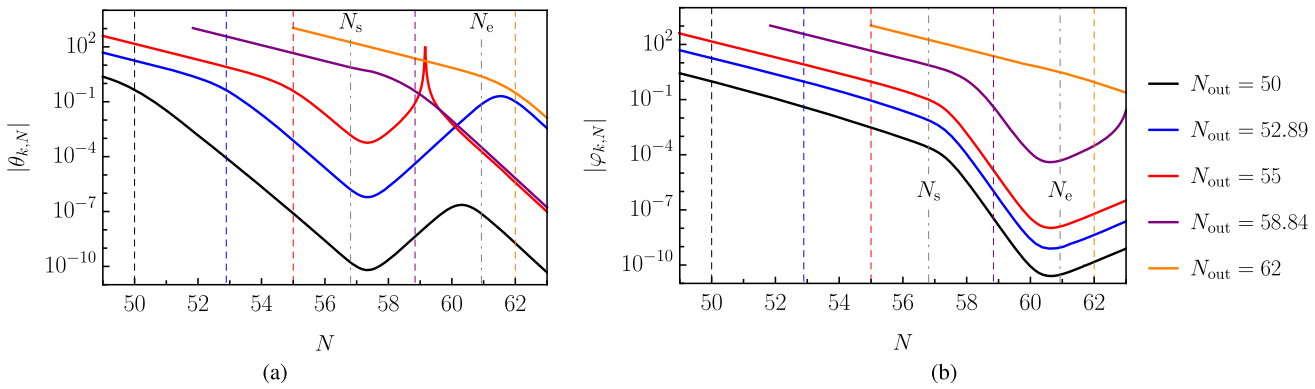

Fig. 8 The evolutions of $|\theta_{k,N}|$ and $|\varphi_{k,N}|$ from $N = 49$ to 63 for five typical scales with different N_{out}. In Fig. 8a, when $N < N_s$, all $|\theta_{k,N}|$ drops, so the angular velocity of $\mathscr{R}_k$ around the origin decreases. When $N > N_s$, this tendency remains for the small-scale cases with $N_{out} = 58.84$ (purple line) and 62 (orange line), so the angular velocity of $\mathscr{R}_k$ keeps decreasing, and $\mathscr{R}_k$ can never be close to the origin. In contrast, for the large-scale cases with $N_{out} = 50$ (black line), 52.89 (blue line), and 55 (red line), $|\theta_{k,N}|$ increases in the USR stage, so $\mathscr{R}_k$ can approach the origin without passing through it. In Fig. 8b, $|\varphi_{k,N}|$ greatly decreases during the USR stage, so φ_k almost keeps constant, confirming the linear evolutions of $\mathscr{R}_k$ in Figs. 4, 5, 6

direction of velocity $\mathscr{R}_{k,N}$, a constant φ_k further confirms the linear evolutions of $\mathscr{R}_k$ in Figs. 4, 5 and 6.

4 Power spectrum in the USR inflation

Now, in Fig. 9, we summarize all our results of the primordial curvature perturbation $\mathscr{R}_k$ in Sect. 3 in the power spectrum $\mathscr{P}_{\mathscr{R}}(k)$. Here, we should mention that, besides $\mathscr{R}_k$, k^3 is also an essential factor that determines the shape of $\mathscr{P}_{\mathscr{R}}(k)$, as shown in Fig. 2a. On the one hand, on large scales (e.g., the pivot scale $k_* = 0.05\ \mathrm{Mpc}^{-1}$ in the Planck satellite experiment), $\mathscr{P}_{\mathscr{R}}(k)$ is nearly scale-invariant with an amplitude of 2.10×10^{-9} [16], because the relevant scales cross the horizon so early that the USR stage has little effect on them. On the other hand, on small scales (e.g., $k > 10^{10}\ \mathrm{Mpc}^{-1}$), the five typical scales are marked as dots with different colors, and several notable features can be found in $\mathscr{P}_{\mathscr{R}}(k)$.

First, there is a high peak up to 0.0222 in $\mathscr{P}_{\mathscr{R}}(k)$ for the scale with $N_{out} = 58.84$. As a result, there can be PBHs of $10^{-17}\ M_\odot$ with the abundance $f_{PBH} \sim 0.1$. This can be understood from Fig. 6, in which the linear evolution of $\mathscr{R}_k$ during the USR stage makes it converge to a position rather far away from the origin and thus enhances $\mathscr{P}_{\mathscr{R}}(k)$ significantly.

Second, the steep growth of $\mathscr{P}_{\mathscr{R}}(k)$ is located around $k \sim 10^{13}\ \mathrm{Mpc}^{-1}$ with $N_{out} \sim 55$, where the scalar spectral index $n_s - 1$ is around 4, in agreement with its theoretical value [31,58,61].

Third, a very noteworthy aspect of $\mathscr{P}_{\mathscr{R}}(k)$ is that there is a sharp dip on the scale with $N_{out} = 52.89$. We attribute the formation of this dip to the linear evolution of $\mathscr{R}_k$ in Fig. 4b. In this situation, $\mathscr{R}_k$ stops at a point extremely near

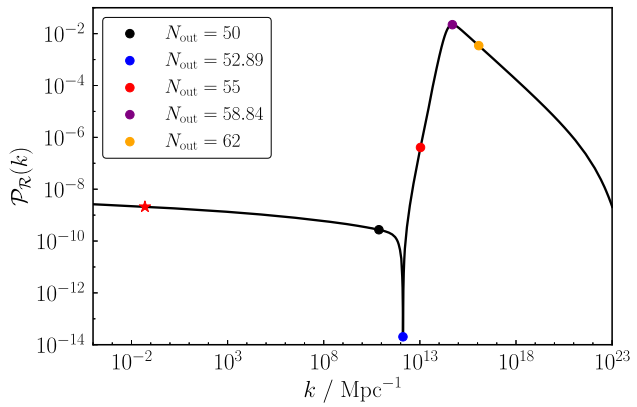

Fig. 9 The power spectrum $\mathscr{P}_{\mathscr{R}}(k)$ in the USR inflation. On large scales, $\mathscr{P}_{\mathscr{R}}(k)$ is nearly scale-invariant with an amplitude of 2.10×10^{-9} (the asterisk denotes the pivot scale $k_* = 0.05\ \mathrm{Mpc}^{-1}$ in the Planck satellite experiment [16]). The five typical scales with different $N_{out} = 50$, 52.89, 55, 58.84, and 62 are marked as dots with different colors. The height of the peak of $\mathscr{P}_{\mathscr{R}}(k)$ reaches 0.0222, corresponding to $N_{out} = 58.84$. The slope of $\mathscr{P}_{\mathscr{R}}(k)$ around $N_{out} \sim 55$ is approximately 4, consistent with its theoretical value [31,58,61]. Moreover, there is a sharp dip in $\mathscr{P}_{\mathscr{R}}(k)$ before its steep growth, with the minimum being 1.61×10^{-14}, corresponding to $N_{out} = 52.89$

the origin, so it greatly decreases $\mathscr{P}_{\mathscr{R}}(k)$ accordingly. Here, we should also point out that, albeit the values of $|\mathscr{R}_k|$ at the end of inflation significantly differ for the scales with $N_{out} = 52.89$, 55, and 58.84, there is no essential difference between them. The unique distinction is the linear evolution of $\mathscr{R}_k$ that converges at quite different final positions.

Last, an interesting issue worth exploring is whether the dip can reach 0 exactly. The answer is actually no. If it could, there must be a special scale, with $\mathscr{R}_k$ located just at the origin at the end of inflation. Therefore, during the linear evolution of $\mathscr{R}_k$ towards the origin, its argument θ_k must be

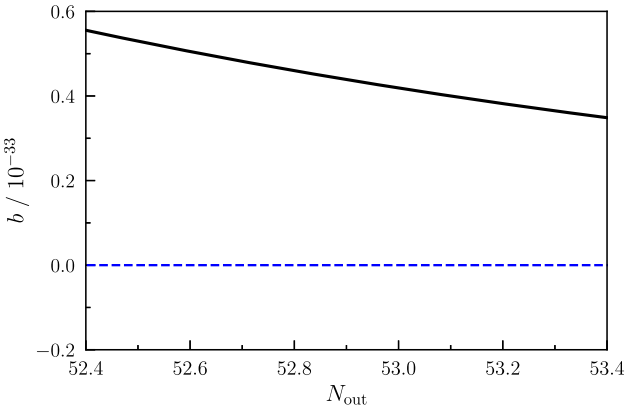

Fig. 10 The intercept b of the linear fit of the real and imaginary parts of $\mathscr{R}_k$ in its linear evolution as a function of $N_{\rm out}$. The positivity of b indicates that the lowest point of the dip in $\mathscr{P}_{\mathscr{R}}(k)$ cannot reach 0 exactly. As the vicinity of the sharp dip is very narrow around $N_{\rm out} = 52.89$, we plot the figure with $N_{\rm out} \in (52.4, 53.4)$ here. (Actually, $b > 0$ even in a large domain from $N_{\rm out} = 51$ to 60.)

a constant, so $\theta_{k,N} = 0$. However, from Eq. (10), $\theta_{k,N}$ can never be 0. Another easy way to clarify this point is to perform a linear fit of the real and imaginary parts of $\mathscr{R}_k$ in its linear evolution and then check whether the intercept b vanishes. If not, $|\mathscr{R}_k|$ is always nonzero, so the dip can never reach 0 exactly. (Even if b vanishes for a special $N_{\rm out}$, we still need to examine whether the linear evolution of $\mathscr{R}_k$ really terminates at the origin or merely passes through it.) In our model, the lowest point of the dip corresponds to $N_{\rm out} = 52.89$. Hence, we plot the intercept b as a function of $N_{\rm out} \in (52.4, 53.4)$ in Fig. 10. We clearly see that b is positive-definite, so it is sufficient to allow us to conclude that the lowest point of the dip is definitely not 0. In fact, the minimum of $\mathscr{P}_{\mathscr{R}}(k)$ is 1.61×10^{-14}, around 10^{-5} that of its pivot value with our model parameters, as shown in Fig. 9.

5 Conclusion

The USR inflation is receiving increasing research interest in recent years. The fundamental reason is that the primordial curvature perturbation $\mathscr{R}_k$ is no longer frozen after the horizon-exit but can still increase significantly, so a notable peak emerges in the power spectrum $\mathscr{P}_{\mathscr{R}}(k)$ on small scales. As a result, there can be abundant PBHs at certain mass windows as an effective candidate of DM and also intensive SIGWs at certain frequencies to be hopefully discovered by the next-generation ground- and space-based detectors.

In this paper, we systematically investigate the evolution of $\mathscr{R}_k$ during the USR inflation and its influence on $\mathscr{P}_{\mathscr{R}}(k)$. Five typical scales with different numbers of e-folds $N_{\rm out}$ when they cross the horizon are investigated in order, which correspond to five typical regions in $\mathscr{P}_{\mathscr{R}}(k)$ (i.e., the nearly scale-invariant region, sharp dip, steep growth, peak, and falling stage, respectively). Our basic conclusions can be summarized as follows.

First, different from previous studies mainly focused on $|\mathscr{R}_k|$ at the end of inflation, we provide an alternative perspective on the entire evolution of $\mathscr{R}_k$ by solving the MS equation in the complex plane. Only in this way can we thoroughly understand the interesting behaviors of $\mathscr{R}_k$ in the revolving process around the origin and the possible linear evolution during the USR stage.

Second, for the very large scale with $N_{\rm out} = 50$ smaller than $N_{\rm s} = 56.81$ or the very small scale with $N_{\rm out} = 62$ larger than $N_{\rm e} = 60.93$, there is only a revolving process around the origin. Therefore, $\mathscr{R}_k$ eventually stops at a position near the origin. For the former, this corresponds to the nearly scale-invariant region of $\mathscr{P}_{\mathscr{R}}(k)$, and for the latter, this corresponds to the falling stage of $\mathscr{P}_{\mathscr{R}}(k)$.

Third, for the moderate scales with $N_{\rm out} = 52.89$, 55, and 58.84 around $N_{\rm s}$, besides the early revolving process, there appears a subsequent linear evolution of $\mathscr{R}_k$ during the USR stage. This means that, different from the fact that the modulus $|\mathscr{R}_k|$ is frozen after the horizon-exit in the usual SR inflation, now it is the argument θ_k that becomes frozen (or with a jump of nearly π), once the scale crosses the horizon in the USR inflation. Nevertheless, $\mathscr{R}_k$ eventually terminates at quite different positions. When $N_{\rm out} = 52.89$, $\mathscr{R}_k$ converges at a position extremely near the origin; when $N_{\rm out} = 58.84$, $\mathscr{R}_k$ converges at a position extremely far away from the origin; the case with $N_{\rm out} = 55$ lies in the middle. In all, these three situations actually stem from the same reason of linear evolution, so they can naturally explain the entire growing stage of $\mathscr{P}_{\mathscr{R}}(k)$ from the dip to the peak.

Fourth, we explore the evolutions of θ_k and φ_k (i.e., the arguments of $\mathscr{R}_k$ and $\mathscr{R}_{k,N}$), which were seldom discussed before. All $|\theta_{k,N}|$ drops before $N_{\rm s}$, but during the USR stage, it decreases for the small-scale cases but increases for the large-scales ones (even with a cusp when $N_{\rm out} = 55$). These behaviors indicate the constancy or a jump of π for θ_k, resulting in the linear evolution of $\mathscr{R}_k$ by the origin but not through it. Moreover, $|\varphi_{k,N}|$ monotonically decreases during the USR stage, and an almost constant φ_k strengthens the conclusion above.

Last, we also discuss whether the lowest point of $\mathscr{P}_{\mathscr{R}}(k)$ can reach 0 exactly. We linearly fit the real and imaginary parts of $\mathscr{R}_k$ and illustrate the intercept b as a function of $N_{\rm out}$ around the dip. It is found that b is positive-definite, so the minimum of $\mathscr{P}_{\mathscr{R}}(k)$ cannot be 0. In fact, this is a general result and can be further verified by looking at the phase diagram in the $\mathscr{R}_k$–$\mathscr{R}_{k,N}$ plane, to be shown elsewhere in our future work.

Altogether, by studying the evolution of the primordial curvature perturbation $\mathscr{R}_k$ in the complex plane, we wish to provide a whole picture and thorough understanding of the

power spectrum $\mathscr{P}_{\mathscr{R}}(k)$ in the USR inflation. This work will be helpful to the model building of the USR inflation and contribute our knowledge of PBH and gravitational wave physics.

Acknowledgements We are very grateful to Gabriele Franciolini, Florian Kühnel, Jing Liu, Shi Pi, Dominik Schwarz, Bing-Yu Su, and Jianing Wang for fruitful discussions. This work is supported by the Fundamental Research Funds for the Central Universities of China (No. N170504015) and the National Training Program of Innovation and Entrepreneurship for Undergraduates (Project S202210145088).

Data Availability Statement This manuscript has no associated data or the data will not be deposited. [Authors' comment: This work is a theoretical study of the evolution of the primordial curvature perturbation in the ultraslow-roll inflation, and no associated data is involved.]

Funded by SCOAP^3. SCOAP^3 supports the goals of the International Year of Basic Sciences for Sustainable Development.

References

1. B.P. Abbott et al. (LIGO Scientific and Virgo Collaboration), Phys. Rev. Lett. **116**, 061102 (2016)
2. S. Bird, I. Cholis, J.B. Muñoz, Y. Ali-Haïmoud, M. Kamionkowski, E.D. Kovetz, A. Raccanelli, A.G. Riess, Phys. Rev. Lett. **116**, 201301 (2016)
3. M. Sasaki, T. Suyama, T. Tanaka, S. Yokoyama, Phys. Rev. Lett. **117**, 061101 (2016)
4. S. Clesse, J. García-Bellido, Phys. Dark Univ. **15**, 142 (2017)
5. A.M. Green, B.J. Kavanagh, J. Phys. G **48**, 043001 (2021)
6. R. Saito, J. Yokoyama, Phys. Rev. Lett. **102**, 161101 (2009)
7. G. Domènech, Universe **7**, 398 (2021)
8. B. Carr, K. Kohri, Y. Sendouda, J. Yokoyama, Rep. Prog. Phys. **84**, 116902 (2021)
9. B. Carr, F. Kühnel, Ann. Rev. Nucl. Part. Sci. **70**, 355 (2020)
10. A. Escrivà, F. Kühnel, Y. Tada, arXiv:2211.05767
11. S. Clesse, J. García-Bellido, Phys. Rev. D **92**, 023524 (2015)
12. M. Castellano et al., Astrophys. J. Lett. **938**, L15 (2022)
13. W.H. Press, P. Schechter, Astrophys. J. **187**, 425 (1974)
14. J.M. Bardeen, J.R. Bond, N. Kaiser, A.S. Szalay, Astrophys. J. **304**, 15 (1986)
15. A.M. Green, A.R. Liddle, K.A. Malik, M. Sasaki, Phys. Rev. D **70**, 041502(R) (2004)
16. N. Aghanim et al. (Planck Collaboration), Astron. Astrophys. **641**, A6 (2020)
17. J. García-Bellido, E.R. Morales, Phys. Dark Univ. **18**, 47 (2017)
18. K. Kannike, L. Marzola, M. Raidal, H. Veermäe, J. Cosmol. Astropart. Phys. **1709**, 020 (2017)
19. C. Germani, T. Prokopec, Phys. Dark Univ. **18**, 6 (2017)
20. H. Motohashi, W. Hu, Phys. Rev. D **96**, 063503 (2017)
21. K. Dimopoulos, Phys. Lett. B **775**, 262 (2017)
22. J.M. Ezquiaga, J. García-Bellido, E.R. Morales, Phys. Lett. B **776**, 345 (2018)
23. G. Ballesteros, M. Taoso, Phys. Rev. D **97**, 023501 (2018)
24. M. Cicoli, V.A. Diaz, F.G. Pedro, J. Cosmol. Astropart. Phys. **1806**, 034 (2018)
25. O. Özsoy, S. Parameswaran, G. Tasinato, I. Zavala, J. Cosmol. Astropart. Phys. **1807**, 005 (2018)
26. I. Dalianis, A. Kehagias, G. Tringas, J. Cosmol. Astropart. Phys. **1901**, 037 (2019)
27. G. Ballesteros, J.B. Jiménez, M. Pieroni, J. Cosmol. Astropart. Phys. **1906**, 016 (2019)
28. S.-L. Cheng, W. Lee, K.-W. Ng, Phys. Rev. D **99**, 063524 (2019)
29. N. Bhaumik, R.K. Jain, J. Cosmol. Astropart. Phys. **2001**, 037 (2020)
30. R. Mahbub, Phys. Rev. D **101**, 023533 (2020)
31. J. Liu, Z.-K. Guo, R.-G. Cai, Phys. Rev. D **101**, 083535 (2020)
32. S.S. Mishra, V. Sahni, J. Cosmol. Astropart. Phys. **2004**, 007 (2020)
33. R.-G. Cai, Z.-K. Guo, J. Liu, L. Liu, X.-Y. Yang, J. Cosmol. Astropart. Phys. **2006**, 013 (2020)
34. D.G. Figueroa, S. Raatikainen, S. Räsänen, E. Tomberg, Phys. Rev. Lett. **127**, 101302 (2021)
35. H.V. Ragavendra, P. Saha, L. Sriramkumar, J. Silk, Phys. Rev. D **103**, 083510 (2021)
36. K.-Y. Choi, S.-B. Kang, R.N. Raveendran, J. Cosmol. Astropart. Phys. **2106**, 054 (2021)
37. K. Kefala, G.P. Kodaxis, I.D. Stamou, N. Tetradis, Phys. Rev. D **104**, 023506 (2021)
38. Y.-C. Liu, Q. Wang, B.-Y. Su, N. Li, Phys. Dark Univ. **34**, 100905 (2021)
39. Q. Wang, Y.-C. Liu, B.-Y. Su, N. Li, Phys. Rev. D **104**, 083546 (2021)
40. I. Dalianis, G.P. Kodaxis, I.D. Stamou, N. Tetradis, A. Tsigkas-Kouvelis, Phys. Rev. D **104**, 103510 (2021)
41. K. Inomata, E. McDonough, W. Hu, Phys. Rev. D **104**, 123553 (2021)
42. S.-L. Cheng, D.-S. Lee, K.-W. Ng, Phys. Lett. B **827**, 136956 (2022)
43. Y.-P. Wu, E. Pinetti, K. Petraki, J. Silk, J. High Energy Phys. **2201**, 015 (2022)
44. K. Inomata, E. McDonough, W. Hu, J. Cosmol. Astropart. Phys. **2202**, 031 (2022)
45. D.G. Figueroa, S. Raatikainen, S. Räsänen, E. Tomberg, J. Cosmol. Astropart. Phys. **2205**, 027 (2022)
46. S. Hooshangi, A. Talebian, M.H. Namjoo, H. Firouzjahi, Phys. Rev. D **105**, 083525 (2022)
47. S.R. Geller, W. Qin, E. McDonough, D.I. Kaiser, Phys. Rev. D **106**, 063535 (2022)
48. G. Franciolini, A. Urbano, Phys. Rev. D **106**, 123519 (2022)
49. S. Balaji, H.V. Ragavendra, S.K. Sethi, J. Silk, L. Sriramkumar, Phys. Rev. Lett. **129**, 261301 (2022)
50. R.N. Raveendran, K. Parattu, L. Sriramkumar, Gen. Relativ. Gravit. **54**, 91 (2022)
51. S.S. Bhatt, S.S. Mishra, S. Basak, S.N. Sahoo, arXiv:2212.00529
52. B.-M. Gu, F.-W. Shu, K. Yang, Y.-P. Zhang, Phys. Rev. D **107**, 023519 (2023)
53. J.-X. Zhao, X.-H. Liu, N. Li, Phys. Rev. D **107**, 043515 (2023)
54. B. Mu, G. Cheng, J. Liu, Z.-K. Guo, Phys. Rev. D **107**, 043528 (2023)
55. H.V. Ragavendra, L. Sriramkumar, Galaxies **11**, 34 (2023)
56. O. Özsoy, G. Tasinato, Universe **9**, 203 (2023)
57. Y. Aldabergenov, S.V. Ketov, Fortsch. Phys. **71**, 2300039 (2023)
58. C.T. Byrnes, P.S. Cole, S.P. Patil, J. Cosmol. Astropart. Phys. **1906**, 028 (2019)
59. P. Carrilho, K.A. Malik, D.J. Mulryne, Phys. Rev. D **100**, 103529 (2019)

60. G. Ballesteros, J. Rey, M. Taoso, A. Urbano, J. Cosmol. Astropart. Phys. **2008**, 043 (2020)
61. G. Tasinato, Phys. Rev. D **103**, 023535 (2021)
62. O. Özsoy, G. Tasinato, Phys. Rev. D **104**, 043526 (2021)
63. O. Özsoy, G. Tasinato, Phys. Rev. D **105**, 023524 (2022)
64. P.S. Cole, A.D. Gow, C.T. Byrnes, S.P. Patil, arXiv:2204.07573
65. A. Karam, N. Koivunen, E. Tomberg, V. Vaskonen, H. Veermäe, J. Cosmol. Astropart. Phys. **2303**, 013 (2023)
66. S. Pi, J. Wang, J. Cosmol. Astropart. Phys. **2306**, 018 (2023)
67. V.F. Mukhanov, Sov. Phys. JETP **68**, 1297 (1988)
68. M. Sasaki, Prog. Theor. Phys. **76**, 1036 (1986)
69. T.S. Bunch, P.C.W. Davies, Proc. R. Soc. Lond. A **360**, 117 (1978)
70. A. Riotto, I.C.T.P. Lect, Notes Ser. **14**, 317 (2003)
71. S. Kachru, R. Kallosh, A.D. Linde, S.P. Trivedi, Phys. Rev. D **68**, 046005 (2003)